J Mater Sci (2014) 49:496–503
DOI 10.1007/s10853-013-7725-7

Roles of alloying additions on local structure and glass-forming ability of Cu–Zr metallic glasses

B. F. Lu · L. T. Kong · Z. Jiang · Y. Y. Huang · J. F. Li · Y. H. Zhou

Received: 18 July 2013 / Accepted: 3 September 2013 / Published online: 17 September 2013
© Springer Science+Business Media New York 2013

Abstract To identify the structural role of alloying element M (M = Ti, Ga, Co, Fe) on the glass-forming ability (GFA) of $Cu_{50}Zr_{50}$ base alloy, the atomic structures of the binary and ternary metallic glasses were examined by extended X-ray absorption fine structure (EXAFS) spectroscopy. The EXAFS curve-fitting analysis indicates that the main structural difference among the metallic glasses is in the atomic packing density of Cu-centered clusters. The relative shortening of the Cu–M distance is closely related to the heat of mixing between Cu and M: the more negative the heat of mixing, the larger is the shortening of the Cu–M distance. Based on a systematic analysis of the component properties and GFA data for Cu–Zr based alloys, it is suggested that alloying elements that bring a more uniform distribution of atomic size and possess strong chemical interactions with the main components should be selected in developing large-size bulk metallic glasses.

Introduction

Alloying addition, as an important technique in traditional metallurgical fields, has also played significant roles in designing and developing bulk metallic glasses (BMGs) with high glass-forming ability (GFA) and desirable properties [1–4]. With the addition of certain amounts of elements such as Y, Ti or Ag, the critical sizes of Cu-, Fe- and Zr-based metallic glasses, which are frequently employed to characterize the GFA of an alloy, can be enhanced from millimeters to centimeters [5–10]. The striking enhancement of the GFA in these alloys is attributed to the alloying effect, which brings the compositions closer to the eutectic points and lowers the alloy liquidus temperature [5–7], consistent with the classical GFA criteria T_{rg} (= T_g/T_l, where T_g is the onset temperature of glass transition and T_l is the liquidus temperature) [11]. It has also been argued that the superior GFA after adding alloying elements was due to the appropriate atomic size mismatch and large negative heat of mixing among constituent elements [6, 9], which enhances local atomic packing efficiency [12].

The enhancement in GFA after adding alloying elements is, however, believed to be a result of modification in the topological and chemical short-to-medium range order of the metallic glasses [13]. Considering that the atomic packing state is closely related to the atomic size (distribution) and chemical affinity of the constituent elements, it is of both fundamental and practical interest to understand how the structure of metallic glasses differs with various alloying elements and how the structure affects the GFA.

Cu–Zr based multi-component BMGs are promising candidates for engineering application because of their relatively high GFA and excellent mechanical properties [14–17]. Understanding the structure–GFA relationship in Cu–Zr based binary and ternary metallic glasses is fundamental to the development of novel BMGs with more complex components. In terms of alloying effect on the local structure, previous works mainly focused on the influence of a given alloying element with different concentrations, for example, the effect of the Be, Ag or Al

B. F. Lu · L. T. Kong · J. F. Li (✉) · Y. H. Zhou
State Key Laboratory of Metal Matrix Composites, School of Materials Science and Engineering, Shanghai Jiao Tong University, Shanghai 200240, People's Republic of China
e-mail: jfli@sjtu.edu.cn

Z. Jiang · Y. Y. Huang
Shanghai Synchrotron Radiation Facility, Shanghai Institute of Applied Physics, Chinese Academy of Sciences, Shanghai 201204, People's Republic of China

content in Cu–Zr based alloys [18–20]. However, the effect of different alloying elements with equal addition level has not been well revealed. In this paper, a simple $Cu_{50}Zr_{50}$ alloy that possesses the highest GFA in the Cu–Zr binary system [21–23] is selected as the base alloy. Alloying elements with various atomic radii, including Ti (1.46 Å), Ga (1.39 Å), Co (1.25 Å) or Fe (1.24 Å) [24], are added to form ternary alloys. Considering that Ti neighbors with Zr in the periodic table, Co and Fe are similar to Cu, and Ga is dissimilar to Zr (1.60 Å) or Cu (1.28 Å), the composition formula of Cu–Zr–M (M = Ti, Ga, Co, or Fe) is designed as $Cu_{50}Zr_{42.5}Ti_{7.5}$, $Cu_{42.25}Zr_{42.25}Ga_{7.5}$, $Cu_{42.5}Zr_{50}Co_{7.5}$ and $Cu_{42.5}Zr_{50}Fe_{7.5}$, respectively. The addition level of alloying element M is selected as 7.5 at.%, based on the considerations that the content of a third element in Cu–Zr based ternary metallic glasses with high GFA is mainly 6–10 at.% [8, 25–28] and that a much smaller content of M may not exert an obvious influence on both structure and GFA.

Experimental

The $Cu_{50}Zr_{50}$ and Cu–Zr–M (M = Ti, Ga, Co, Fe) master alloy ingots were prepared by arc melting a designed mixture of pure Zr (99.9 %), Cu (99.99 %), Ti (99.99 %), Ga (99.99 %), Co (99.99 %) and Fe (99.99 %) in a Ti-gettered high-purity argon atmosphere. The alloy ingots were remelted five times to ensure homogeneity. Amorphous ribbons with a thickness of ~40 μm were produced from the master alloy ingots using the single-roller melt-spinning technique. Wedge-shaped samples were obtained by casting the alloy melts into a wedge-shaped Cu mold with an included angle of 10°.

The amorphous nature of the as-quenched ribbons was identified using a Thermo ARL X-ray diffractometer (XRD) with monochromatic Cu Ka radiation. The local structure of the ribbons was examined by X-ray absorption fine structure (XAFS) spectroscopy. XAFS measurements were performed at the beamline BL14W1 of the Shanghai Synchrotron Radiation Facility (SSRF, Shanghai, China), where the electron beam energy is 3.5 GeV and the beam current is 140–210 mA. The incident X-rays were monochromatized by an Si (111) double-crystal monochromator. Zr K-edge and Cu K-edge EXAFS spectra for all samples were collected in transmission mode at ambient temperature. The energy calibration was performed using standard Zr and Cu foils. The thicknesses of the samples were optimized to obtain suitable absorption jumps at each K-absorption edge.

EXAFS data analysis was performed using the IFEFFIT version 1.2.9 [29]. The EXAFS spectra were extracted using Athena, and weighted by a weighting factor k^n ($n = 3$) based on the element types of absorbing and scattering atoms in Cu–Zr system and the signal-to-noise ratio of $\chi(k)$ spectra. Then, they were Fourier transformed (FT) into real space through a Hanning window (3.1–11.1 $Å^{-1}$ for Cu K-edge and 3.1–11.0 $Å^{-1}$ for Zr K-edge). EXAFS fits were performed in k-space after filtering out the selected region of coordination shells through a Hanning window (1.6–2.8 Å for Cu K-edge and 1.75–3.25 Å for Zr K-edge) and back Fourier transforming (BFT) into k-space. To reduce the number of degrees of freedom, a coordination constraint, $N_{Zr-Cu} + N_{Zr-Zr} = 14$, was applied during the fitting procedure for Cu–Zr–M metallic glasses at the Zr K-edge. The theoretical scattering amplitudes and phases were calculated by a code FEFF 6L [30]. The coordination number information of $Cu_{33}Zr_{67}$ metallic glass in Ref. [20] was used to fit the EXAFS spectra of the $Cu_{33.3}Zr_{66.7}$ metallic glass (a composition very near to $Cu_{33}Zr_{67}$) in this work at the Cu and Zr K-edge. The resultant amplitude reduction factor S_0^2 values are 0.31 for Cu and 0.40 for Zr. Based on the chemical transferability of S_0^2, the structure information of the $Cu_{50}Zr_{50}$ and Cu–Zr–M metallic glasses were obtained through EXAFS curve fitting.

Results and discussion

Critical thickness of glass formation

Figure 1 illustrates the critical thickness for glass formation in $Cu_{50}Zr_{50}$ and Cu–Zr–M (M = Ti, Ga, Co, Fe) wedge-shaped samples. The critical thickness for glass formation was measured by observing the microstructure on the longitudinal section of the wedge-shaped sample under an optical microscopy and a scanning electronic microscopy. Such a method has been verified to be feasible before [23]. For each composition, at least three wedge-shaped samples were used to verifying the GFA. It can be seen that the additions of different alloying elements result in different GFA. The addition of 7.5 at.% Ti to $Cu_{50}Zr_{50}$ improves the GFA, while adding the same amount of Ga, Co or Fe sequentially degrades the GFA.

EXAFS oscillations and their Fourier transforms

Figure 2 shows the XRD patterns of the as-quenched Cu–Zr–M ribbons. One sees clearly that each pattern consists of a broad diffraction peak without any detectable sharp Bragg peaks, indicating an amorphous structure. The amorphous nature of the as-quenched $Cu_{50}Zr_{50}$ ribbon has been confirmed in our previous work [23].

To identify the origin of the alloying addition effects on the GFA of the Cu–Zr alloys, EXAFS experiments of these

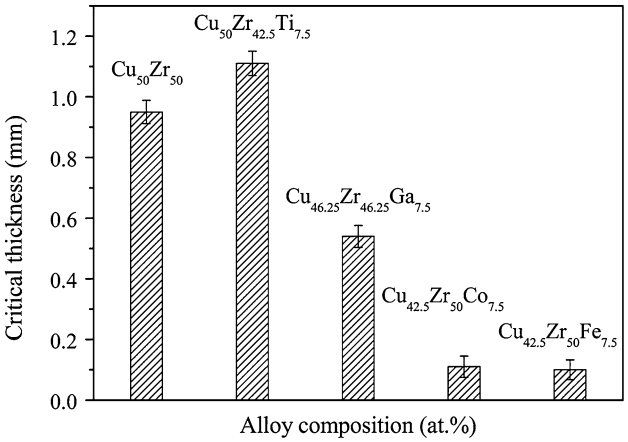

Fig. 1 Critical thickness for glass formation in $Cu_{50}Zr_{50}$ and Cu–Zr–M wedge-shaped samples

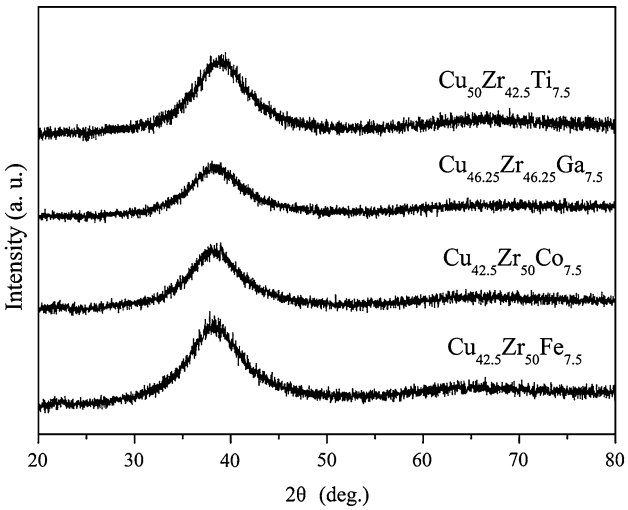

Fig. 2 XRD patterns of Cu–Zr–M ribbons

glassy ribbons were performed. Figure 3a, b illustrates the normalized and k^3-weighted EXAFS data at the Cu and Zr K-edge, respectively. Modules of Fourier transforms (FTs) of corresponding EXAFS signals in Fig. 3a, b are displayed in Fig. 3c, d, respectively. To suppress the low R peaks, the cutoff distance, Rbkg, should be large enough. On the other hand, a too large value of Rbkg will damage the data. In the present work, the value of Rbkg was 1.15 Å for Cu K-edge and 1.41 Å for Zr K-edge.

Curve-fitting analysis

To obtain the more quantitative structural parameters around the core-excited Cu and Zr atoms in the $Cu_{50}Zr_{50}$ and Cu–Zr–M metallic glasses, the curve-fitting analysis of the measured EXAFS spectra was carried out. For Cu K-edge, the first neighbor peaks are back Fourier transformed into k-space in the ranges of $R = 1.6$–2.8 Å; for Zr K-edge, the first and second nearest neighbor peaks are treated ($R = 1.75$–3.25 Å). The resultant Fourier-filtered $\chi(q)$ data are presented in Fig. 4 in the form of solid lines.

For $Cu_{50}Zr_{50}$ metallic glass, noticing the dominant icosahedral clusters revealed by molecular dynamic (MD) simulations [31], it is believed that the corresponding Cu-centered Cu_6Zr_7 icosahedral short range order (ISRO) may prevail around Cu atoms in $Cu_{50}Zr_{50}$ amorphous sample. For Cu–Zr–M metallic glasses, Cu-centered Cu_6Zr_7 icosahedral clusters with Cu or Zr atom substituted by alloying elements M are therefore constructed as initial structure models to fit the experimental $\chi(q)$ spectra at the Cu K-edge. Whether M substitutes Cu or Zr atom depends on the atomic size similarity and the chemical interaction between M and the main constituent Cu and Zr. Based on this criterion, Zr is substituted by Ti for Cu–Zr–Ti, while Cu is replaced by Ga, Co and Fe for Cu–Zr–Ga, Cu–Zr–Co and Cu–Zr–Fe, respectively. Similarly, using the average partial coordination number N_{Zr-Cu}, N_{Zr-Zr} obtained from X-ray and neutron diffraction technique for Ref. [32], Zr-centered Zr_8Cu_7 clusters with Cu or Zr substituted by alloying elements M are created as initial structural models to fit the experimental $\chi(q)$ data at the Zr K-edge. As shown in Fig. 4a, b, the calculated spectra are in good agreement with the experimental ones both for Zr K-edge and Cu K-edge.

The local structure of Cu–Zr–M metallic glasses

As presented by the curve-fitting results, adding a third element M to $Cu_{50}Zr_{50}$ metallic glasses does not obviously alter the dominant structure features of Cu- and Zr-centered clusters. However, modification of the local structure is expected and should be reflected in the interatomic distance and coordination numbers.

It is known that the peak position in a (partial) radical distribution functions (RDF) corresponds to the average distance (R) between the central atom and the neighboring atoms and the area underneath the main peak of RDF reflects the average number of nearest neighbors (N). As pointed out in previous works [32, 33], the structural features of Cu–Zr metallic glasses can be better understood from the perspective of Cu-centered clusters. Correspondingly, the magnified RDF of $Cu_{50}Zr_{50}$ and Cu–Zr–M metallic glasses at the Cu K-edge are further compared, as presented in Fig. 5. There exist subtle but distinct differences in the position of the main peak and the areas underneath it. Taking $Cu_{50}Zr_{50}$ as a reference (solid line), it is clear that the addition of Ti, Ga leads to a higher peak intensity and a left shift in the peak position; the addition of Co results in comparable peak intensity, but a slight left shift in the peak position; the addition of Fe corresponds to a lower peak intensity, but basically unchanged peak

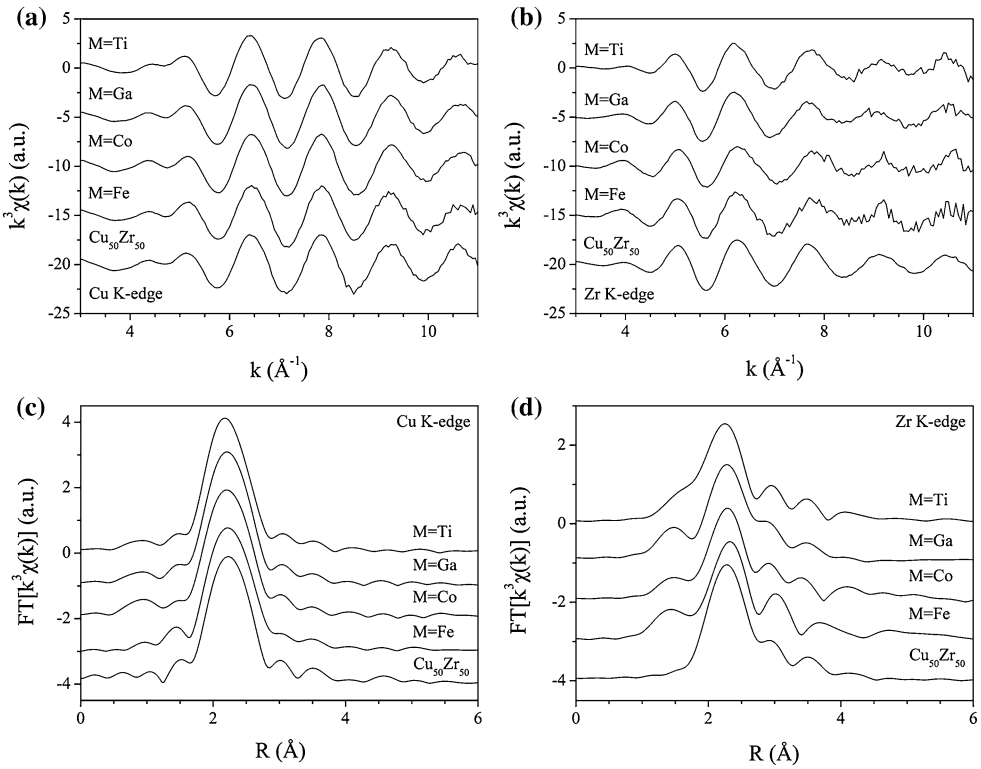

Fig. 3 **a** and **b** $k^3\chi(k)$ EXAFS spectra of $Cu_{50}Zr_{50}$ and Cu–Zr–M metallic glasses at Cu K-edge and Zr K-edge; **c** and **d** RDF obtained via Fourier transforms of (**a**) and (**b**), respectively. The *gray dotted vertical lines* are guidance for eyes

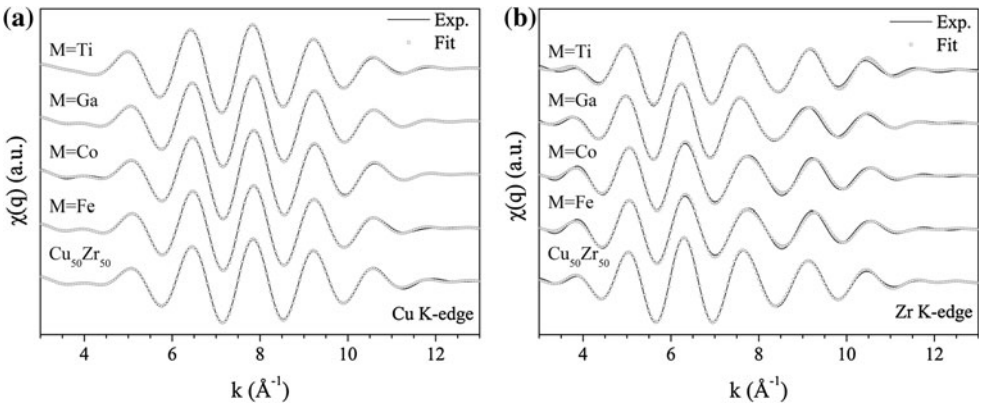

Fig. 4 χ(q) experimental spectra and best-fit results at the Cu K-edge (**a**) and Zr K-edge (**b**) for $Cu_{50}Zr_{50}$ and Cu–Zr–M metallic glasses. The *solid lines* denote the experimental spectra, while the *scattered circles* represent the fitting spectra

position. In other words, Cu atoms possesses the highest coordination number N_{Cu} and the smallest average neighboring distance R_{Cu} in Cu–Zr–Ti metallic glass; a higher N_{Cu} and smaller R_{Cu} in Cu–Zr–Ga metallic glass; a comparable N_{Cu} and smaller R_{Cu} in Cu–Zr–Co metallic glass; and a relatively lower N_{Cu} and almost invariable R_{Cu} in Cu–Zr–Fe metallic glass. The structural parameters obtained by curve fitting at the Cu K-edge, including R_{i-j}, N_{i-j} and σ^2_{i-j} (mean squared relative disorder), are summarized in Table 1, where i and j denote the central and neighboring atoms, respectively. Combining the information on R_{Cu} and N_{Cu}, it is easy to see that the atomic packing density of the Cu-centered clusters decreases sequentially from $Cu_{50}Zr_{42.5}Ti_{7.5}$, $Cu_{42.25}Zr_{42.25}Ga_{7.5}$, $Cu_{42.5}Zr_{50}Co_{7.5}$ and $Cu_{50}Zr_{50}$ to $Cu_{42.5}Zr_{50}Fe_{7.5}$.

The curve-fitting results for the Zr K-edge are summarized in Table 2. One finds that the Zr–Cu, Zr–Zr interatomic distances (R_{Zr-Cu}, R_{Zr-Zr}) are almost constant (being 2.70 Å and 3.10–3.11 Å, respectively) except in the Cu–Zr–Fe alloy, where increased R_{Zr-Cu} (2.72 Å) and R_{Zr-Zr} (3.15 Å) are observed. This means that adding Ti, Ga or Co results in almost invariable atomic packing density, while adding Fe leads to a slightly decreased atomic packing density since the coordination number N_{Zr} remains unchanged.

The interatomic distances for Cu–Ti, Zr–Ti, Zr–Ga, Zr–Co and Zr–Fe obtained from the curve fitting in this work are consistent with the previous results obtained via EXAFS experiments or MD simulations [34–39]. For example, R_{Cu-Ti} in Cu–Zr–Ti metallic glass is 2.55 Å in the

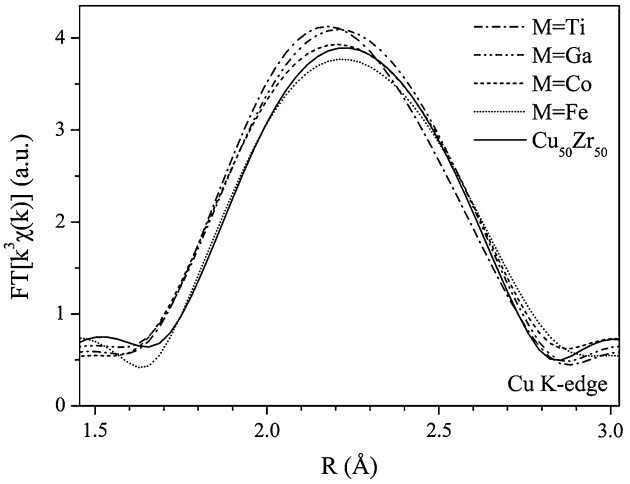

Fig. 5 Enlargement of the main peaks of RDF obtained via Fourier transforming $k^3\chi(k)$ EXAFS spectra for $Cu_{50}Zr_{50}$ and Cu–Zr–M metallic glasses at the Cu K-edge

Table 1 Fitting results including interatomic distance R_{i-j}, (partial) coordinate number N_i (N_{i-j}) and mean-squared relative disorder σ^2_{i-j} for Cu K-edge of $Cu_{50}Zr_{50}$ and Cu–Zr–M metallic glasses ($\Delta R_{i-j} = \pm 0.01$ Å, $\Delta N_{i-j} = \pm 0.5$, $\Delta\sigma^2_{i-j} = \pm 0.002$ Å^2)

Composition	Atomic pair	R_{i-j} (Å)	N_{i-j}	N_{Cu}	σ^2_{i-j} (Å^2)
$Cu_{50}Zr_{50}$	Cu–Cu	2.50	4.8	11.7	0.010
	Cu–Zr	2.71	6.9		0.016
M = Ti	Cu–Cu	2.48	5.1	12.3	0.012
	Cu–Zr	2.71	6.2		0.014
	Cu–Ti	2.55	1.0		0.008
M = Ga	Cu–Cu	2.47	4.8	12.3	0.009
	Cu–Zr	2.71	6.7		0.015
	Cu–Ga	2.57	0.8		0.005
M = Co	Cu–Cu	2.50	4.3	12.1	0.013
	Cu–Zr	2.71	7.1		0.014
	Cu–Co	2.46	0.7		0.004
M = Fe	Cu–Cu	2.50	4.1	11.5	0.015
	Cu–Zr	2.72	6.7		0.013
	Cu–Fe	2.46	0.7		0.003

present work, quite close to those (2.56 and 2.57 Å) obtained by curve fitting of the EXAFS spectra of the Cu–Ti binary and Zr–Ti–Cu–Ni quaternary metallic glasses [38, 39]. This indicates that the resultant interatomic distances for Cu–Zr–M metallic glasses are physically reasonable.

Factors affecting the GFA of Cu–Zr–M alloys

From the perspective of atomic diffusion and crystallization kinetics in undercooled liquid, alloys with relatively dense atomic packing usually possess high GFA.

Table 2 Fitting results including interatomic distance R_{i-j}, (partial) coordinate number N_i (N_{i-j}), and mean-squared relative disorder σ^2_{i-j} for Zr K-edge of $Cu_{50}Zr_{50}$ and Cu–Zr–M metallic glasses ($\Delta R_{i-j} = \pm 0.01$ Å, $\Delta N_{i-j} = \pm 0.5$, $\Delta\sigma^2_{i-j} = \pm 0.002$ Å^2)

Composition	Atomic pair	R_{i-j} (Å)	N_{i-j}	N_{Zx}	σ^2_{i-j} (Å^2)
$Cu_{50}Zr_{50}$	Zr–Cu	2.70	6.7	14.0	0.011
	Zr–Zr	3.10	7.3		0.016
M = Ti	Zr–Cu	2.70	6.7	14.0	0.011
	Zr–Zr	3.11	6.3		0.016
	Zr–Ti	2.95	1.0		0.007
M = Ga	Zr–Cu	2.70	6.4	14.0	0.010
	Zr–Zr	3.11	6.5		0.016
	Zr–Ga	2.84	1.1		0.006
M = Co	Zr–Cu	2.70	5.7	14.0	0.015
	Zr–Zr	3.11	7.3		0.018
	Zr–Co	2.66	1.0		0.007
M = Fe	Zr–Cu	2.73	5.7	14.0	0.012
	Zr–Zr	3.15	7.3		0.017
	Zr–Fe	2.65	1.0		0.008

Meanwhile, the atomic packing state is closely related to the atomic size distribution of the constituent elements. Actually, theoretical studies have revealed that a wider standard deviation of sphere radii (atomic radii) will result in a higher packing density [40], while experimental investigations on Y- and Ca-based alloys have shown a significant effect of atomic size distribution on GFA [41].

The atomic radius distribution of components and the experimental GFA data for Cu–Zr–M and other typical Cu–Zr based multi-component alloys are summarized in Table 3. According to the atomic size distribution feature, the alloying elements in Cu–Zr based alloys can be categorized into three groups: (1) Ni, Co and Fe belongs to a group (denoted by M_1) since their tabulated radii (1.25, 1.25, 1.24 Å) fall out of the atomic size distribution gap between Cu and Zr and close to the atomic radius of Cu (1.28 Å); (2) Ti, Ga, Al and Ag belong to another group (denoted by M_2) as their radii (1.47, 1.39 1.43, 1.44 Å) are between the atomic radii of Zr and Cu; (3) Be (1.13 Å) is classified as the third group (denoted by M_3) because its atomic radius is not between the atomic radii of Zr and Cu, but much smaller than that of Cu. With the fact that the Cu–Zr–M_2 (M_3) alloys show much larger GFAs than the Cu–Zr–M_1 alloys, it is clear that the GFA in Cu–Zr–M alloys is closely related to the uniformity of the atomic size distribution of the main constitute Cu, Zr and the third element M. The Cu–Zr based alloys with more components have more uniform atomic size distributions and therefore possess much better GFAs. As shown in Table 3, the addition of Al with an intermediate size into Cu–Zr–M_1 (M_1 = Fe, Ni) results in a dramatic improvement of GFA.

Adding medium-size Al and small-size Be into Cu–Zr–M_2 (M_2 = Ag) leads to the formation of 73 mm BMG. This further validates the importance of a more uniform and wider atomic distribution in improving the atomic packing density and GFA for Cu–Zr multi-component alloys.

Apart from the atomic size distribution, the chemical interaction between the alloying element M and the main component Cu and Zr also influences the local atomic structure of Cu–Zr–M metallic glasses. The stronger the interatomic bonding (chemical affinity) is, the higher the diffusion activation energy, which increases the difficulty for atoms to rearrange in supercooled liquid and promotes the glass formation. As mentioned in Sect. The local structure of Cu–Zr–M metallic glasses, the addition of 7.5 at.% Ga or Co into $Cu_{50}Zr_{50}$ results in higher atomic packing, but lower GFA. We believe that the decrease in GFA after the addition of Ga and Co is related to the chemical affinity between the alloying element M and the main component Cu, since Cu-centered clusters can reflect the dominant structural features. To address this issue, the interatomic distances of the Cu–M obtained from curve fitting of EXAFS spectra (R_{i-j}) and that calculated as the sum of Goldschmidt atomic radii (R^0_{i-j}) are listed in Table 4. The value of $(R^0_{i-j} - R_{i-j})/R^0_{i-j}$, which denotes the relative distance shortening, is calculated and also listed in Table 4, together with the heat of mixing for the corresponding Cu–M atomic pairs. The actual Cu–Ti interatomic distance (2.55 Å) is noticeably shorter than the sum (2.74 Å) of their Goldschmidt atomic radii. The relative shortening reaches 6.9 %, comparable to that of Al–Cu in Cu–Zr–Al metallic glasses (~6 %) [51, 52]. However, the relative shortening of other Cu–M (M = Ga, Co, or Fe) is much smaller, varying from 3.7, 2.8 to 2.4 %, sequentially. Interestingly, such a variation in relative shortening displays a strong correlation with the heat of mixing between Cu and M, that is, −9, +1, +6 and +13 kJ/mol for Cu–Ti, Cu–Ga, Cu–Co and Cu–Fe, respectively [53]. The repulsive interaction between Cu–Ga and Cu–Co atomic pairs resulting from their positive heat of mixing may reduce the stability of Cu-centered clusters in the liquid and in turn lower the GFA of Cu–Zr–Ga and Cu–Zr–Co. For Cu–Zr–Fe alloy, the lower atomic packing density in the metallic glass and the more repulsive interaction between Cu–Fe atomic pairs weaken the atomic bonding, resulting in a poor GFA. The analyses above suggest that selecting alloying elements that bring both uniform atomic size distribution and strong chemical interaction with the main components are vital to achieve high GFA.

Conclusions

The effects of adding alloying element M (M = Ti, Ga, Co, Fe) on the atomic structure and GFA of $Cu_{50}Zr_{50}$ metallic glass have been investigated by EXAFS spectroscopy and wedge casting technique. Compared to the $Cu_{50}Zr_{50}$ base alloy, the addition of 7.5 at.% Ti enhances the GFA, while adding equivalent other elements such as Ga, Co or Fe sequentially deteriorate the GFA. Among the $Cu_{50}Zr_{50}$ and Cu–Zr–M metallic glasses, the atomic packing density of the Cu-centered clusters decreases sequentially from

Table 3 Summary of atomic radius distribution of components (with the largest in front) and critical sizes for glass formation in Cu–Zr based metallic glasses with various alloying elements (highlighted using bold fonts)

Composition (at.%)	Atomic radius for each component (Å)	Critical size (mm)	References
$Cu_{50}Zr_{42.5}$**Ti**$_{7.5}$	1.60, **1.46**, 1.28	1.11 (wedge)	This work
$Cu_{46.25}Zr_{46.25}$**Ga**$_{7.5}$	1.60, **1.39**, 1.28	0.54 (wedge)	This work
$Cu_{42.5}Zr_{50}$**Co**$_{7.5}$	1.60, 1.28, **1.25**	0.11 (wedge)	This work
$Cu_{42}.Zr_{505}$**Fe**$_{7.5}$	1.60, 1.28, **1.24**	0.10 (wedge)	This work
$Cu_{20}Zr_{70}$**Ni**$_{10}$	1.60, 1.28, **1.25**	0.06 (ribbon)	[42]
$Cu_{46}Zr_{46}$**Al**$_8$	1.60, **1.43**, 1.28	ϕ7	[27]
$Cu_{45}Zr_{48}$**Al**$_7$		ϕ8	[25]
$Cu_{40}Zr_{50}$**Ag**$_{10}$	1.60, **1.44**, 1.28	ϕ5	[8]
$Cu_{45}Zr_{45}$**Ag**$_{10}$		ϕ6	[26]
$Cu_{25}Zr_{50}$**Be**$_{25}$	1.60, 1.28, **1.13**	≥ϕ8	[43]
$Cu_{30}Zr_{55}$**Ni**$_5$**Al**$_{10}$	1.60, **1.43**, 1.28, **1.25**	ϕ30	[44]
$Cu_{25}Zr_{60}$**Fe**$_5$**Al**$_{10}$	1.60, **1.43**, 1.28, **1.24**	ϕ20	[45]
$Cu_{36}Zr_{48}$**Ag**$_8$**Al**$_8$	1.60, **1.44**, **1.43**, 1.28	ϕ25	[46]
		>ϕ20	[9]
$Cu_{43}Zr_{43}$**Al**$_7$**Be**$_7$	1.60, **1.43**, 1.28, **1.13**	ϕ12	[47]
$Zr_{41.2}$**Ti**$_{13.8}$$Cu_{12.5}$**Ni**$_{10}$**Be**$_{22.5}$	1.60, **1.46**, 1.28, **1.25**, **1.13**	ϕ25	[48, 49]
$Zr_{46}Cu_{30.14}$**Al**$_8$**Ag**$_{8.36}$**Be**$_{7.5}$	1.60, **1.44**, **1.43**, 1.28, **1.13**	ϕ73	[50]

Table 4 Comparison between the interatomic distances of Cu–M pairs R_{i-j} obtained from curve fitting of the EXAFS spectra and that calculated as the sum of the nominal (Goldschmidt) atomic radii R^0_{i-j}

Atomic pairs	Interatomic distances		$(R^0_{i-j} - R_{i-j})/R^0_{i-j}$ (%)	$\Delta H^{\text{mix}}_{i-j}$ (KJ/mol)
	R_{i-j} (Å)	$R^0_{\text{i-j}}$ (Å)		
Cu–Ti	2.55	2.74	−6.9	−9
Cu–Ga	2.57	2.67	−3.7	+1
Cu–Co	2.46	2.53	−2.8	+6
Cu–Fe	2.46	2.52	−2.4	+13

The value of $(R^0_{i-j} - R_{i-j})/R^0_{i-j}$ reflects the degree of distance shortening, while $\Delta H^{\text{mix}}_{ij}$ represents the heat of mixing between elements i and j

$Cu_{50}Zr_{42.5}Ti_{7.5}$, $Cu_{42.25}Zr_{42.25}Ga_{7.5}$, $Cu_{42.5}Zr_{50}Co_{7.5}$ and $Cu_{50}Zr_{50}$ to $Cu_{42.5}Zr_{50}Fe_{7.5}$. For Zr-centered clusters, adding Ti, Ga or Co results in almost invariable atomic packing density, while adding Fe leads to a decreased atomic packing density. The relative shortening of Cu–M distance is closely related to the heat of mixing between Cu and M: the more negative the heat of mixing, the larger is the relative shortening of the Cu–M distance. According to the atomic size distribution feature, the alloying elements in Cu–Zr based ternary alloys can be categorized into three groups: Cu–Zr–M_1 (M_1 = Co, Fe, Ni) alloys possess less uniform atomic size distribution; Cu–Zr–M_2 (M_2 = Ti, Al, Ga, Ag) and Cu–Zr–M_3 (M_3 = Be) alloys exhibit more uniform atomic size distribution. Cu–Zr–M_1 alloys possess low GFA, whereas Cu–Zr–M_2 and Cu–Zr–M_3 alloys show relatively high GFA. In summary, the GFA of Cu–Zr–M metallic glass is affected by both the local atomic packing density and chemical interaction between the alloying element M and the main components.

Acknowledgements The authors thank the Shanghai Synchrotron Radiation Facility in Shanghai for the use of the synchrotron radiation facilities (Grants No. 10sr0345 and 11sr0250). Financial supports from the National Natural Science Foundation of China (Grants No. 51071103 and 50831003) and the National Basic Research Program of China (Grant No. 2011CB610405) are gratefully acknowledged.

References

1. Lu ZP, Liu CT (2004) J Mater Sci 39:3965. doi:10.1023_B_JMSC.0000031478.73621.64
2. Wang WH (2007) Prog Mater Sci 52:540
3. Xu Y, Wang Y, Liu X, Chen G, Zhang Y (2009) J Mater Sci 44:3861. doi:10.1007/s10853-009-3511-y
4. Zhou W, Kong LT, Li JF, Zhou YH (2012) J Mater Sci 47:4996. doi:10.1007/s10853-012-6375-5
5. Lu ZP, Liu CT, Thompson JR, Porter WD (2004) Phys Rev Lett 92:245503
6. Xu DH, Duan G, Johnson WL (2004) Phys Rev Lett 92:245504
7. Ma D, Cao H, Ding L, Chang YA, Hsieh KC, Pan Y (2005) Appl Phys Lett 87:171914
8. Zhang W, Jia F, Zhang Q, Inoue A (2007) Mater Sci Eng, A 459:330
9. Jiang QK, Wang XD, Nie XP, Zhang GQ, Ma H, Fecht HJ, Bednarcik J, Franz H, Liu YG, Cao QP, Jiang JZ (2008) Acta Mater 56:1785
10. Hua N, Pang S, Li Y, Wang J, Li R, Georgarakis K, Yavari AR, Vaughan G, Zhang T (2011) J Mater Res 26:539
11. Turnbull D (1969) Contemp Phys 10:473
12. Inoue A (2000) Acta Mater 48:279
13. Cheng YQ, Ma E (2011) Prog Mater Sci 56:379
14. Gilbert CJ, Ritchie RO, Johnson WL (1997) Appl Phys Lett 71:476
15. Kawashima A, Kurishita H, Kimura H, Zhang T, Inoue A (2005) Mater Trans 46:1725
16. He Q, Cheng YQ, Ma E, Xu J (2011) Acta Mater 59:202
17. Wang X, Cao QP, Chen YM, Hono K, Zhong C, Jiang QK, Nie XP, Chen LY, Wang XD, Jiang JZ (2011) Acta Mater 59:1037
18. Park ES, Chang HJ, Kim DH (2008) Acta Mater 56:3120
19. Fujita T, Konno K, Zhang W, Kumar V, Matsuura M, Inoue A, Sakurai T, Chen MW (2009) Phys Rev Lett 103:075502
20. Antonowicz J, Pietnoczka A, Zalewski W, Bacewicz R, Stoica M, Georgarakis K, Yavari AR (2011) J Alloys Comp 509:S34
21. Tang MB, Zhao DQ, Pan MX, Wang WH (2004) Chin Phys Lett 21:901
22. Li Y, Guo Q, Kalb JA, Thompson CV (2008) Science 322:1816
23. Lu BF, Li JF, Kong LT, Zhou YH (2011) Intermetallics 19:1032
24. Senkov ON, Miracle DB (2001) Mater Res Bull 36:2183
25. Wang D, Tan H, Li Y (2005) Acta Mater 53:2969
26. Duan G, De Blauwe K, Lind ML, Schramm JP, Johnson WL (2008) Scripta Mater 58:159
27. Yu HB, Wang WH, Bai HY (2010) Appl Phys Lett 96:081902
28. Zhang Y, Mattern N, Eckert J (2012) J Alloys Comp 514:141
29. Ravel B, Newville M (2005) J Synchrotron Radiat 12:537
30. Rehr JJ, Albers RC (2000) Rev Mod Phys 72:621
31. Sha ZD, Xu B, Shen L, Zhang AH, Feng YP, Li Y (2010) J Appl Phys 107:063508
32. Ma D, Stoica AD, Wang XL, Lu ZP, Xu M, Kramer M (2009) Phys Rev B 80:014202
33. Cheng YQ, Sheng HW, Ma E (2008) Phys Rev B 78:014207
34. Ikeda T, Matsubara E, Waseda Y, Inoue A, Chang T, Masumoto T (1995) Mater Trans 36:1093
35. Hui X, Liu X, Gao R, Hou H, Fang H, Liu Z, Chen G (2008) Sci China, Ser G 51:400
36. Huang L, Wang CZ, Hao SG, Kramer MJ, Ho KM (2010) Phys Rev B 81:014108
37. Kaban I, Jovari P, Stoica M, Mattern N, Eckert J, Hoyer W, Beuneu B (2010) J Phys Condens Mat 22:404208
38. Machado KD, Maciel GA, Sanchez DF, de Lima JC, Jovari P (2010) Solid State Commun 150:1674
39. Mechler S, Schumacher G, Koteski V, Riesemeier H, Schaefers F, Mahnke HE (2010) Appl Phys Lett 97:041914
40. He D, Ekere NN, Cai L (1999) Phys Rev E 60:7098
41. Guo FQ, Poon SJ, Shiflet GJ (2005) J Appl Phys 97:013512
42. Wang HR (2002) J Alloys Comp 347:101
43. Duan G, Lind ML, De Blauwe K, Wiest A, Johnson WL (2007) Appl Phys Lett 90:211901

44. Inoue A, Zhang T (1996) Mater Trans 37:185
45. Zhang QS, Zhang W, Inoue A (2009) Scripta Mater 61:241
46. Zhang W, Zhang Q, Qin C, Inoue A (2008) Mater Sci Eng, B 148:92
47. Kim YC, Lee JC, Cha PR, Ahn JP, Fleury E (2006) Mater Sci Eng, A 437:248
48. Peker A, Johnson WL (1993) Appl Phys Lett 63:2342
49. Busch R, Kim YJ, Johnson WL (1995) J Appl Phys 77:4039
50. Lou HB, Wang XD, Xu F, Ding SQ, Cao QP, Hono K, Jiang JZ (2011) Appl Phys Lett 99:051910
51. Cheng YQ, Ma E, Sheng HW (2009) Phys Rev Lett 102:245501
52. Wang CC, Wong CH (2012) J Alloys Comp 510:107
53. Takeuchi A, Inoue A (2005) Mater Trans 46:2817